Topological Stability and Self-Association of a Completely Hydrophobic Model Transmembrane Helix in Lipid Bilayers†

Yoshiaki Yano,‡ Tomokazu Takemoto,§ Satoe Kobayashi,§ Hiroyuki Yasui,|| Hiromu Sakurai,|| Wakana Ohashi,⊥ Miki Niwa,⊥ Shiroh Futaki,⊥ Yukio Sugiura,⊥ and Katsumi Matsuzaki*,‡

Graduate School of Biostudies and Graduate School of Pharmaceutical Sciences, Kyoto University, Sakyo-ku, Kyoto 606-8501, Japan, Institute for Chemical Research, Kyoto University, Uji, Kyoto 611-0011, Japan, and Department of Analytical and Bioinorganic Chemistry, Kyoto Pharmaceutical University, Yamashina-ku, Kyoto 607-8414, Japan

Received June 5, 2001; Revised Manuscript Received December 17, 2001

ABSTRACT: Investigation of interactions between hydrophobic model peptides and lipid bilayers is perhaps the only way to elucidate the principles of the folding and stability of membrane proteins (White, S. H., and Wimley, W. C. (1998) *Biochim. Biophys. Acta 1367*, 339−352). We designed the completely hydrophobic "inert" peptide modeling a transmembrane (TM) helix without any of the specific side-chain interactions expected, X-$(LALAAAA)_3$-NH_2 [X = Ac (**I**), 7-nitro-2-1,3-benzoxadiazol-4-yl (**II**), or 5(6)-carboxytetramethylrhodamine (**III**)]. Fourier transform infrared-polarized attenuated total reflection measurements revealed that **I** as well as **II** assume a TM helix in hydrated 1-palmitoyl-2-oleoyl-*sn*-glycero-3-phosphocholine bilayers. Dithionite quenching experiments detected no topological change (flip-flop) in the helix **II** for at least 24 h. Thus, the TM helix itself is a highly stable structure, even in the absence of flanking hydrophilic or aromatic amino acids which are suggested to play important roles in stable TM positioning. Helix self-association in lipid bilayers was detected by fluorescence resonance energy transfer between **II** and **III**. The peptide was in a monomer−antiparallel dimer equilibrium with an association free energy of ∼−13 kJ/mol. Electron spin resonance spectra of 1-palmitoyl-2-stearoyl-(14-doxyl)-*sn*-glycero-3-phosphocholine demonstrated the presence of a motionally restricted component at lower temperatures.

Elucidation of the physical principles of the folding and the stability of proteins is not only one of the central issues in biophysics but also important for the prediction of protein structures from sequence data in the post-genomic era. As compared with water-soluble proteins, the folding fundamentals of membrane proteins (MPs)[1] remain mostly unknown, although the thermodynamic steps to their folded (or equilibrium) states have been clearly conceptualized (*1*−*3*). Aqueous and membrane environments significantly differ in physicochemical properties (*1*). For example, the lipidic milieu with a low dielectric constant greatly strengthens the electrostatic interactions, whereas it nullifies hydrophobic interactions, which are, in contrast, quite important in water.

Investigation of the interactions between hydrophobic model peptides and lipid bilayers is an attractive approach to this MP folding problem because it can overcome many difficulties accompanied with treating MPs, such as the resistance of MPs against complete denaturation and their intractability due to insolubility (*4*). One can directly obtain thermodynamic parameters regarding, for example, insertion of a helix into a lipid bilayer and side-chain interactions between adjacent helices. In fact, an increasing number of model studies oriented toward MPs have been carried out. Most studies so far reported used hydrophobic sequences composed of ∼20 amino acids, which can form transmembrane (TM) helices flanked by a few charged residues (typically lysine) to increase solubility and stabilize TM positioning (*5*−*8*). However, to detect relatively weak helix−helix interactions in lipid bilayers, these peptides may not be appropriate because electrostatic repulsion between charged residues tends to hamper the association of these peptides. Therefore, we propose that an "inert" completely hydrophobic peptide even without aromatic amino acids, the interfacial location of which is considered to stabilize TM positioning (*2*, *9*, *10*), is essential as a starting point in a series of systematic studies to experimentally determine

† Supported in part by the Mitsubishi Foundation, the Kato Memorial Bioscience Foundation, and Grant-in-Aid for Scientific Reserch for Advanced Area (A-13024244) from the Ministry of Education, Culture, Sports, Science and Technology of Japan.

* To whom correspondence should be addressed. Phone: 81-75-753-4574. Fax: 81-75-761-2698. E-mail: katsumim@pharm.kyoto-u.ac.jp.

‡ Graduate School of Biostudies, Kyoto University.

§ Graduate School of Pharmaceutical Sciences, Kyoto University.

|| Kyoto Pharmaceutical University.

⊥ Institute for Chemical Research, Kyoto University.

[1] Abbreviations: ESR, electron spin resonance; FRET, fluorescence resonance energy transfer; Fmoc, 9-fluorenylmethoxycarbonyl; FTIR−PATR, Fourier transform infrared-polarized attenuated total reflection; LUVs, large unilamellar vesicles; MLVs, multilamellar vesicles; MP, membrane protein; NBD, 7-nitro-2-1,3-benzoxadiazol-4-yl; NBD−PE, 1,2-dipalmitoyl-*sn*-glycero-3-phosphoethanolamine-*N*-(7-nitro-2-1,3-benzoxadiazol-4-yl); POPC, 1-palmitoyl-2-oleoyl-*sn*-glycero-3-phosphocholine; RP-HPLC, reversed-phase high-performance liquid chromatography; 14-SLPC, 1-palmitoyl-2-stearoyl-(14-doxyl)-*sn*-glycero-3-phosphocholine; TFE, 2,2,2-trifluoroethanol; TM, transmembrane; TMR, 5(6)-carboxytetramethylrhodamine; TMR−PE, *N*-(6-tetramethylrhodaminethiocarbamoyl)-1,2-dihexadecanoyl-*sn*-glycero-3-phosphoethanolamine triethylammonium salt.

10.1021/bi011161y CCC: $22.00
Published on Web 02/08/2002

thermodynamic parameters related to helix−helix and helix−lipid interactions. Such a peptide would faithfully report the intrinsic properties of TM helices, and when used as a host peptide, it would reveal the roles of various amino acids in the stability of TM orientation and helix−helix interactions. Indeed, polyalanines (*11*−*13*) and polyalanines attached to a soluble carrier protein (*14*) have been used in computational and experimental studies, respectively.

For the first time, we report the behavior of a completely inert hydrophobic peptide modeling a TM helix in lipid bilayers. The 21-residue peptide, X-$(LALAAAA)_3$-NH_2 [X = Ac (**I**), 7-nitro-2-1,3-benzoxadiazol-4-yl (NBD) (**II**), or 5(6)-carboxytetramethylrhodamine (TMR) (**III**)], is exclusively composed of helix-promoting leucine and alanine, and the terminal charges were blocked by acetylation and amidation. If the entire sequence forms an α helix, the length (ca. 3 nm) almost matches the hydrophobic thickness of 1-palmitoyl-2-oleoyl-*sn*-glycero-3-phosphocholine (POPC), a representative phospholipid in mammalian cell membranes. No specific side-chain interactions, such as ion pair, hydrogen bond, or leucine zipper based on heptad repeats (*15*), are expected. The fluorescent probe NBD was introduced at the N-terminus to estimate helix topology and the location of the N-terminus using a quenching reaction with membrane-impermeable dithionite ions (*16*) and polarity-sensitive position of maximum, respectively. Peptide aggregation was estimated on the basis of self-quenching of **II** and fluorescence resonance energy transfer (FRET) from **II** to **III**. We found that even this simplest of helices can form a topologically stable TM helix and self-aggregates in the lipid matrix.

MATERIALS AND METHODS

Materials. A peptide chain was constructed by 9-fluorenylmethyloxycaronyl (Fmoc) solid-phase synthesis on a Rink amide resin. TMR, NBD, and acetyl moieties were introduced at the N-terminus with 5(6)-carboxytetramethylrhodamine-*N*-hydroxysuccinimide ester, NBD-Cl, and acetic anhydride in the presence of diisopropylethylamine, respectively. The peptide resin was treated with trifluoroacetic acid-ethanedithiol (95:5) followed by purification by reversed-phase high-performance liquid chromatography (RP-HPLC). The purities of the peptides (>90%) were confirmed by RP-HPLC, amino acid analysis, and ion-spray mass spectroscopy. POPC was obtained from Sigma (St. Louis, MO). Spectrograde chloroform and methanol were products of Nacalai Tesque (Kyoto, Japan). NMR grade 2,2,2-trifluoroethanol (TFE) was purchased from Aldrich (Milwaukee, WI). 1,2-Dipalmitoyl-*sn*-glycero-3-phosphoethanolamine-*N*-(7-nitro-2-1,3-benzoxadiazol-4-yl) (NBD−PE) and 1-palmitoyl-2-stearoyl-(14-doxyl)-*sn*-glycero-3-phosphocholine (14-S-LPC) were supplied by Avanti Polar Lipids (Alabaster, AL). *N*-(6-Tetramethylrhodaminethiocarbamoyl)-1,2-dihexadecanoyl-*sn*-glycero-3-phosphoethanolamine triethylammonium salt (TMR−PE) was obtained from Molecular Probes (Eugene, OR). The lipids and the peptides were dissolved in chloroform and methanol or TFE, respectively. The lipid concentration was determined in triplicate by phosphorus analysis (*17*). The concentrations of the fluorophore-labeled peptides were determined on the basis of extinction coefficients in methanol (ϵ_{449} = 20 000 M^{-1} for **II** and ϵ_{544} = 103 000 M^{-1} for **III**), which were obtained by absorbance combined with quantitative amino acid analysis in duplicate.

Fourier Transform Infrared-Polarized Attenuated Total Reflection (FTIR−PATR) Spectroscopy. Oriented films of POPC/peptide were prepared by uniformly spreading a chloroform/TFE solution (0.5 mL) of 10 mM POPC/0.1 mM peptide on a germanium ATR plate (80 × 10 × 4 mm) followed by gradual evaporation of the solvent. The last traces of the solvent were removed under vacuum overnight. The films were hydrated with a D_2O-soaked piece of filter paper put over the plate for 3 h. Hydration was estimated to be 30 w/w % by the intensity ratio of the OD stretching band of D_2O to the antisymmetric CH_2 stretching band of POPC (*18*). The film thickness of about 6 μm, estimated from the applied amount of the lipid was much larger than the depth of penetration of the evanescent wave (0.2−0.8 μm) in the range 3000−800 cm^{-1}. To minimize spectral contributions of atmospheric water vapor, the instrument was purged with dry N_2 gas. FTIR−PATR measurements were carried out on a BioRad FTS-3000MX spectrometer equipped with a Hg−Cd−Te detector and a PIKE horizontal ATR attachment and an AgBr polarizer. The total reflection number was 10 on the film side. The spectra were measured at a resolution of 2 cm^{-1} and an angle of incidence of 45° and derived from 256 co-added interferograms with the Happ−Genzel apodization function. The subtraction of the gently sloping water vapor was carried out to improve the background prior to frequency measurement. The dichroic ratio, R, defined by $\Delta A_{||}/\Delta A_{\perp}$, was calculated from the polarized spectra. The absorbance (ΔA) was obtained either as the peak height for the CH_2 symmetric stretching vibration band or as the area for the amide bands. The subscripts || and ⊥ refer to polarized light with its electric vector parallel and perpendicular to the plane of incidence, respectively. For ATR correction, refractive indexes of 4.003 and 1.440 were used for germanium and the sample film, respectively.

Vesicle Preparation. Large unilamellar vesicles (LUVs) were prepared by an extrusion method, as described elsewhere (*16*). Briefly, a lipid/peptide mixed film, after drying under vacuum overnight, was hydrated with Tris-HCl buffer (10 mM Tris/150 mM NaCl/1 mM EDTA (pH 7.4)) and vortex-mixed to produce multilamellar vesicles (MLVs). The suspension was subjected to 10 freeze−thaw cycles and then extruded through polycarbonate filters (0.1-μm pore size filters, 31 times).

Detection of Peptide Topology. External addition of dithionite to LUVs chemically quenches the NBD groups in the outer leaflets of the bilayers. Inner leaflet-labeled vesicles were prepared by reacting 2.4 mM POPC LUVs containing 0.5 mol % NBD-labeled peptide with 50 mM sodium dithionite/50 mM Tris for 3 min at room temperature. The vesicles were immediately separated from dithionite by gel filtration (Bio-Gel A-1.5m, 1.5 × 18 cm column). The inside labeled LUVs were incubated for various times at 25 °C. After 20 μL of 1 M sodium dithionite/1 M Tris had been added to 2 mL of the sample, NBD fluorescence was monitored at excitation and emission wavelengths of 450 and 533 nm, respectively, on a Shimadzu RF-5000 spectrofluorometer at 25 °C.

Detection of FRET Efficiency. FRET efficiency (E_T) or relative quantum yield ($Q_r = 1 - E_T$) was determined by the degree of NBD (donor) fluorescence quenching. Briefly, LUVs containing a donor and an acceptor were prepared as described previously, and the donor fluorescence was

compared with that of LUVs without the acceptor. Background fluorescence intensity (caused mainly by lipid vesicle scattering) was subtracted when it was larger than 1%. Corrected emission spectra in the range 480−650 nm were obtained with quinine sulfate as a reference (*19*). Fluorophore concentration was precisely determined on the basis of absorbance after dissolving the vesicles with 10 times the volume of methanol.

E_T was calculated by

$$E_T = 1 - Q_r = 1 - (F_{icor}/F_0)(A_0{}^{+MeOH}/A^{+MeOH}) \quad (1)$$

F_{icor} and F_0 denote the donor fluorescence intensities in LUVs with or without the acceptor, respectively. A^{+MeOH} and $A_0{}^{+MeOH}$ express donor absorbances at the absorption maximum in methanol (455 nm). F_{icor} was corrected for the inner filter effect

$$F_{icor} = F_i \times 10^{0.5bA_{\lambda em}} \quad (2)$$

F_i represents the measured fluorescence intensity. The path length of the cuvette in centimeters is denoted by b. $A_{\lambda em}$ expresses the acceptor absorbance at the emission wavelength.

FRET Theory. E_T is related to the inverse sixth power of the distance (R) between the donor and the acceptor in an isolated donor−acceptor system (*20*)

$$R = R_0(E_T{}^{-1} - 1)^{1/6} \quad (3)$$

R_0 (Å) is called the Förster distance

$$R_0 = (9.8 \times 10^3)(J\kappa^2 Q_D n^{-4})^{1/6} \quad (4)$$

Q_D, n, and κ^2 are the quantum yield of the donor in the absence of acceptor, the refraction index of the medium, and the dipole−dipole orientation factor, respectively. If the donor and the acceptor are randomly oriented with each other, as frequently assumed, $\kappa^2 = {}^2/_3$. J, the spectral overlap integral, is given by

$$J = \frac{\int_0^\infty A(\lambda)E(\lambda)\lambda^4 \, d\lambda}{\int_0^\infty E(\lambda) \, d\lambda} \quad (5)$$

$A(\lambda)$ is the absorbance spectrum of the acceptor (M^{-1} cm^{-1}) as a function of wavelength, λ, and $E(\lambda)$ is the corrected fluorescence emission spectrum of the donor. These spectra were measured in LUVs containing 0.5 mol % fluorescent probes. $A(\lambda)$ was determined after subtraction of the corresponding background transmittance spectrum. Under our experimental conditions, the estimated apparent absorbance loss originating from vesicle light scattering was less than 3%, which had little influence on the evaluation of R_0. The donor quantum yield (Q_D) in the vesicles was determined with NBD−PE in ethanol as a reference (*21*).

Calculation of Association Free Energy from FRET Data. In lipid bilayers, spontaneous FRET between a donor and randomly distributed acceptors, as well as FRET due to donor−acceptor association, contribute to the observed Q_r value

$$Q_r = (1 - f_b)q_s + f_b q_a \quad (6)$$

Of all the donor molecules, the fraction of donors aggregated with acceptors is denoted by f_b. Relative quantum yields due to spontaneous transfer and aggregation are expressed by q_s and q_a, respectively. q_a was assumed to be 0 (see Results). q_s was estimated by (see Appendix)

$$q_s = \left(\frac{1}{q_{cis}} + \frac{1}{q_{trans}} - 1\right)^{-1} \quad (7)$$

q_{cis} and q_{trans} represent the relative quantum yields due to spontaneous transfers in the cis and trans leaflets, respectively, which were evaluated by the analysis of Wolber and Hudson (*22*). The required parameters in this analysis were R_0, donor−acceptor closest approach, and two-dimensional acceptor concentration (per unit area). The surface area per lipid was assumed to be 60 Å^2. The donor−acceptor closest approaches of the peptides on the cis and trans sides were evaluated to be 12.5 and 42.5 Å, respectively, on the basis of fluorophore molecular diameters and helix orientation. In the case of the fluorescent lipid (TMR−PE), the closest approaches (cis, 12.5 Å; trans, 39.0 Å) were calculated using the distance of the fluorophore from the bilayer center determined by the parallax method (19.5 Å) (*23*). The fraction of aggregated peptides (f_a) can be calculated by eq 8, assuming a monomer−n-mer equilibrium and the binomial distribution of donor and acceptor in the n-mer (*24*), because the oligomer without any acceptors does not contribute to FRET

$$f_b = f_a(1 - P_d{}^{n-1}) \quad (8)$$

P_d denotes the fraction of donor in the donor−acceptor mixture. The association constant (K_n) and corresponding standard Gibbs free-energy change (ΔG_n) are given by

$$\Delta G_n = -RT \ln K_n \quad (9)$$

$$K_n = \frac{[M_n]}{[M]^n} \quad (10)$$

R and T represent the gas constant and the absolute temperature, respectively. [M_n] and [M] denote the mole fractions of n-mer and monomer in the bilayers, respectively. The experiments were performed at sufficiently low peptide concentrations, expecting an ideal dilution regime

$$[M] = (1 - f_a)\frac{2n_p}{2n_p + n_l} \quad (11)$$

$$[M_n] = \frac{2f_a n_p}{n(2n_p + n_l)} \quad (12)$$

The moles of peptide and lipid are denoted by n_p and n_l, respectively. The factor of 2 is introduced to take the TM nature of the peptide into consideration.

Electron Spin Resonance (ESR). POPC MLVs (4 mM) containing 1.5 mol % 14-SLPC with or without 2 mol % **II** were prepared and subjected to 10 freeze−thaw cycles. The sample was packed in a 10 μL Drummond hematocrit capillary tube. ESR spectra were recorded on an X-band ESR spectrometer JES−RE−1X (JEOL; Tokyo, Japan) equipped with nitrogen gas flow variable-temperature regulation.

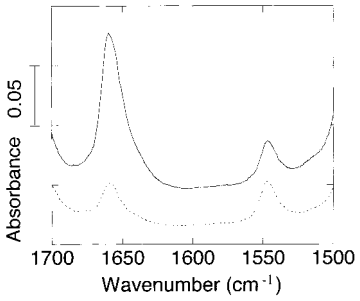

FIGURE 1: FTIR−PATR amide region spectra of a D_2O hydrated **I**/POPC (1/100) film for the IR beam with its electric vector parallel (—) and perpendicular (- - -) to the plane of incidence, at ambient temperature (~25 °C).

Table 1: FTIR−PATR Parameters of **I** in POPC Bilayers[a]

band	frequency (cm^{-1})	R^b	θ (deg)[c]	α (deg)[d]
amide **I**	1659.6 ± 0.2	4.8 ± 0.05	35	16 ± 1
amide **II**	1546.9 ± 0.2	0.9 ± 0.03	88	10 ± 4

[a] Errors indicate standard deviations of two independent measurements. [b] Dichroic ratio. [c] Angles between the transition moment and the helix axis (*28*). [d] Mean orientation angle of the helix around the membrane normal calculated from the *R* value (*29*).

Instrumental conditions were as follows: microwave frequency, 9.24 GHz at 5 °C and 9.40 GHz at 25 °C; microwave power, 5.0 mW; field modulation frequency, 100 kHz; modulation amplitude width, 0.1 mT; magnetic field scan, 10 mT; scanning time, 4 min; receiver gain, 250; response time, 0.3 s. The spectrometer was calibrated with an Advantest Microwave Counter R5372 (Tokyo, Japan). The central magnetic field was adjusted to coincide with the field of the second spectral signal due to the nitroxide radical using Mn (II) doped in MnO ($\Delta H_{3-4} = 8.69$ mT) as a standard. ESR spectral data were collected and analyzed with an ESR Data Analyzer WIN−RAD (Radical Research; Tokyo, Japan). The ESR spectrometer's analogue signal was converted to the digital mode by the ESR Data Analyzer and then input to a memory device.

RESULTS

FTIR−PATR. FTIR−PATR spectroscopy is useful for simultaneously determining the conformations and orientations of both peptides and lipids without perturbation. Figure 1 shows PATR spectra of D_2O-hydrated **I**/POPC (1/100) films in the region 1500−1700 cm^{-1}. The wavenumbers of maximal intensity of the amide I and II bands are listed in Table 1, indicating that the peptide assumed a helical structure (*25*, *26*). Both peaks were narrow with half-widths of ~15 cm^{-1}, suggesting that the entire peptide assumed an almost pure helix without major contributions from any other secondary structures. The dichroic ratio can be used to determine the orientation of the transition dipoles and, therefore, the molecular axis (*27*). Using the known angles, θ, between the helix axis and the transition moments (*28*), the helix orientation angle, α, was calculated (*29*) and is summarized in Table 1

$$\cos^2 \alpha = \frac{1}{3}\left(\frac{4}{3\cos^2 \theta - 1}\frac{R - 2.00}{R + 1.45} + 1\right) \qquad (13)$$

The angles less than 20° clearly demonstrate that the helix spanned the bilayer. The amide I/amide II area ratio (3.0 ± 0.06) did not change upon hydration (data not shown), suggesting that the helix, which was embedded in the hydrocarbon core of the membrane, suffered from no H/D exchange (*27*). Several bands assignable to lipid functional groups (CH_2 symmetric stretching, C═O stretching, PO_2^- antisymmetric stretching, N−CH_3 antisymmetric stretching) did not show any noticeable changes in the presence of the peptide (data not shown). Similar results were also obtained for **II** (data not shown). These results did not depend on the peptide concentrations studied (1−2 mol %).

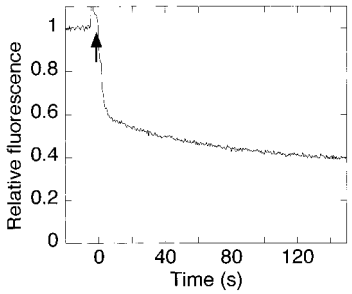

FIGURE 2: Topology determination by NBD-dithionite reaction. Sodium dithionite was added to POPC LUVs (200 μM) containing 0.5 mol % **II** at the time indicated by the arrow (final concentration 10 mM). Fluorescence at 533 nm was monitored at an excitation wavelength of 450 nm at 25 °C.

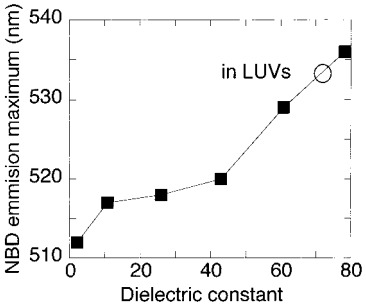

FIGURE 3: Dependence of wavelength of maximal intensity on medium polarity. NBD fluorescence spectra of **II** (1 μM) were measured in various dioxane/water mixtures with different dielectric constants at 25 °C. The open circles denote the position of maximum in POPC LUVs.

Helix Topology. The topology of the helix was examined on the basis of the quenching of the NBD group with membrane-impermeable dithionite ions (*30*). Figure 2 shows that the addition of the ions to POPC LUVs containing 0.5 mol % **II** reduced the fluorescence intensity by 50% within seconds, indicating that half of the peptide molecules assumed an N-terminal-outside topology. The gradual subsequent decrease in fluorescence suggests that the dithionite ion was slowly permeable across the peptide-containing membrane.

The wavelength of maximal intensity of NBD fluorescence is highly dependent on the polarity of its environment. NBD fluorescence spectra of **II** were measured in various dioxane/water mixtures. Figure 3 plots the position of maximum as a function of the dielectric constant of the medium.[2] The position of maximum of **II** in POPC bilayers was 533 nm before and after dithionite addition, suggesting that (1) the fluorophore was located at a rather polar environment of the

[2] The peptide **II** was practically insoluble and formed aggregates in water. However, the fluorescence spectrum could be measured, and its position of maximal was most blueshifted.

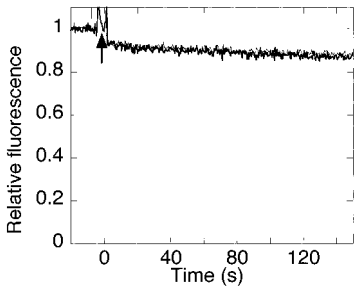

FIGURE 4: Flip-flop of **II** in POPC LUVs. Inner-labeled LUVs were prepared by treating POPC LUVs containing 0.5 mol % **II** with dithionite. Dithionite was again added as in Figure 2 after incubation of the inner-labeled vesicles for 15 min (- - -) and 25 h (—) at 25 °C.

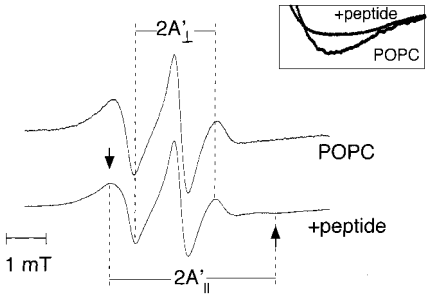

FIGURE 5: ESR spectra of 14-SLPC in the presence (lower) or the absence (upper) of 2 mol % **II** at 5 °C. $2A_{||}'$ and $2A_{\perp}'$ show the outer and inner hyperfine splittings, respectively. (Inset: expanded spectra (high field region) at 25 °C.)

membrane (effective dielectric constant ~70), in keeping with the TM orientation and (2) there were only two populations of TM helices with different topologies. We also compared the position of maximum with that of NBD−PE in POPC LUVs, because no simple correlation of the position of maximum may not be expected with the solvent dielectric constant considering the rather complex photochemistry of NBD (*31*). The NBD group of NBD−PE is known to locate approximately at the level of the phosphate group (*32*). The position of maximum of NBD−PE (522 nm) was more blueshifted as compared with **II**, suggesting that the NBD group of the peptide existed in a more polar environment.

The topological stability of **II** was also estimated using the dithionite method. The fraction of the flopped NBD-labeled peptide was quantitated by adding sodium dithionite after incubation of the inside-labeled vesicles for 15 min and 25 h (Figure 4) (*16*). No exposure of the NBD group was observed, even after a 25 h incubation, suggesting that the flip-flop of the helix did not occur on a timescale of a day.

ESR. ESR spectra of the spin-labeled lipids provide information on the peptide−lipid interactions. The ESR spectra measured at 5 °C are shown in Figure 5. Pure POPC with 14-SLPC in the fluid lamellar phase was characterized by a spectrum with three sharp peaks. In the presence of the peptide **II** (2 mol %), a second, motionally restricted component (so-called boundary lipid component) was observed in the outer wings of the central three-line components (arrows), suggesting that the peptide affected the mobility of the surrounding lipid chains. This second component was more readily detected in the high field region. Lipid order parameter, *S*, was calculated according to Subczynski et al. (*5*) from maximum splitting of ESR spectra. Measured $A_{||}'$ and $A_{\perp}'$ values were 1.55 and 1.01 mT for pure lipid and

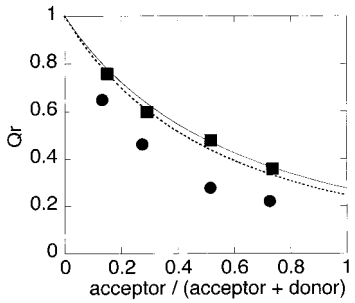

FIGURE 6: Detection of peptide aggregation using FRET at 25 °C. Q_r values of **II**−TMR−PE pair (■) and **II**−**III** pair (●) were measured at a peptide/lipid mole ratio of 0.007. Theoretical spontaneous transfer curves of the **II**−TMR−PE pair (—) and **II**−**III** pair (- - -) were calculated according to Wolber and Hudson (*22*).

2.05 and 0.99 mT for the boundary lipid components, respectively. The calculated order parameter value of the boundary lipid component (0.43) was obviously larger than that of pure lipid (0.25). At 25 °C, the two components were more averaged (inset), probably because the exchange rate of spin-labeled lipids between the two components was comparable to the ESR timescale (~10^{-9} s) (*33*).

Helix Association in Lipid Bilayers. FRET was used to determine the helix−helix interaction thermodynamics in the lipid bilayers. NBD and TMR were selected as an energy donor−acceptor pair and attached to the N-terminus of the peptide because the R_0 value for this pair (~50 Å) was greater than the interchromophore distance, even in the antiparallel association. We made the commonly used simple assumption that one TMR per aggregate completely quenches the fluorescence of all NBD molecules in the same oligomer (*34*). Spontaneous FRET originating from the random distribution of the acceptors in two dimensions was experimentally estimated using a TMR-labeled lipid as an acceptor. With $\kappa^2 = {}^2/_3$, the R_0 values were calculated to be 50.6 and 54.1 Å for the **II**−TMR−PE and the **II**−**III** pairs, respectively. Figure 6 shows the observed Q_r values as a function of acceptor mole fraction at a constant peptide/lipid ratio of 0.007. For the **II**−TMR−PE pair, the observed values were well explained by the Wolber−Hudson equation, guaranteeing that parameters such as R_0, closest approach, and lipid surface area were reasonably selected. For the **II**−**III** pair, the observed Q_r values were significantly lower than the theoretical spontaneous transfer curve, suggesting peptide aggregation. To evaluate the association thermodynamics, FRET measurements were carried out at various peptide/lipid ratios. Figure 7A plots the association free energy against the peptide concentration assuming monomer−oligomer equilibria. The monomer−dimer equilibrium gave almost constant association free-energy values (12.9 ± 0.8) kJ/mol over the measured peptide concentration range, which was limited to <0.7 mol % expecting an ideal dilution regime. Figure 7B plots the fraction of dimer as a function of the peptide concentration. The observed values were well explained by the theoretical prediction.

Helix Orientation in Dimer. To obtain information on the structure of the dimer, self-quenching of **II** in the lipid bilayers was examined. The fluorescence of NBD-labeled lipids in membranes is known to be self-quenched at higher concentrations (*35*). If the N-terminus fluorophores in the dimer are close to each other, as expected in a parallel dimer,

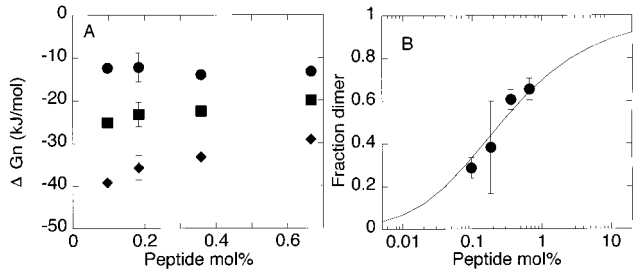

FIGURE 7: Thermodynamics of peptide self-association at 25 °C. (A) Association Gibbs free energies were calculated from the observed Q_r values at a donor−acceptor mole ratio of 1/0.4 assuming monomer−dimer (●), monomer−trimer (■), and monomer−tetramer (◆) equilibrium, respectively. (B) Fraction dimer was plotted as a function of peptide mole fraction (●). The curve is a theoretical one with $\Delta G_2 = -12.9$ kJ/mol.

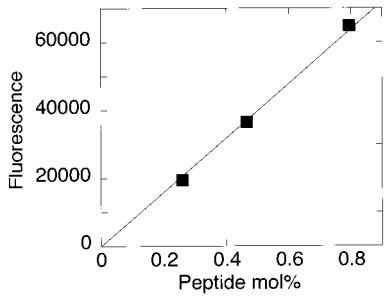

FIGURE 8: Absence of self-quenching of **II**. Fluorescence intensity defined as emission peak area in the range 480−650 nm is plotted as a function of peptide mol % in POPC LUVs at 25 °C.

self-quenching may be observed. Figure 8 shows that no self-quenching was observed in the peptide concentration range of significant dimerization (Figure 7), suggesting an antiparallel association of the helices.[3]

DISCUSSION

TM Helices. The FTIR−PATR and fluorescence measurements demonstrate that our model peptides stably form TM helices in POPC bilayers (Figures 1−3 and Table 1). The attachment of the NBD group at the N-terminus did not affect the conformation or the orientation of the helix. The wavenumber of maximal intensity of the amide I band (1660 cm^{-1}) was several wavenumbers larger than those of typical α helices. Similar observations were reported for representative TM helicies of bacteriorhodopsin (*36*, *37*) and alamethicin (*37*). Slight derivations from normal $\alpha_{||}$-type structures may exist as proposed for bacteriorhodopsin (*38*). The presence of a 3_{10} helix is unlikely because the amide II frequency of this structure is around 1532 cm^{-1} (*39*).

The free energy of insertion of a TM helix is determined by the unfavorable free energy of dehydrating the peptide backbone and the favorable free energy associated with side-chain partitioning (*2*, *40*, *41*). Therefore, the amino acid composition of the buried TM segment is important to overall TM stability. Recently, it was reported that polyalanine-based helices did not form stable TM helices (*42*, *43*), indicating that six hydrophobic leucine residues in our peptides contribute to the stabilization of the TM helices.

[3] The NBD fluorescence of a leucine zipper-forming TM helix exhibited self-quenching, suggesting a parallel association (Yano et al., unpublished work).

On the basis of X-ray structures of MPs, flanking hydrophilic or aromatic amino acids are considered to play important roles in stable TM positioning (*2*, *8*−*10*). Indeed, model TM peptides with their "stabilizing" residues at both ends of the hydrophilic stretches were confirmed to orient almost parallel to the bilayer normal by FTIR−PATR (*6*), oriented CD (*10*), and fluorescence quenching (*7*). Our results clearly show that the inert hydrophobic sequence with a helical length matching the hydrophobic thickness of the lipid bilayer is enough for the formation of an orientationally stable TM helix. Indeed, not all TM helices in MPs have these stabilizing residues.

Topological Stability. Surprisingly, the flip-flop study (Figure 4) indicates that the TM helix **II** without any polar residues is topologically very stable. These results also reject the possibility of apparent flip-flop due to redistribution of the helix through the aqueous phase, in keeping with the practical insolubility of the helix. The introduction of the NBD group never suppresses the flip-flop motion because NBD labeling greatly accelerates the flip-flop of a phospholipid (*16*). There have been very few studies on helix flip-flop in lipid bilayers. NMR (*44*), and theoretical (*45*) studies evaluated the flip-flop rate of alamethicin in POPC bilayers to be 10^{-7} to 10^{-6} s^{-1}, in accordance with our study. Honig's group calculated the energetics of insertion of the $(Ala)_{25}$ helix into a model bilayer of 3 nm thickness (*12*). The free-energy difference between the TM helix and the helix completely embedded in the bilayer center with the helical axis perpendicular to the bilayer normal (a transition state of helix flip-flop) was estimated to be 8−40 kcal/mol, depending on the degree of capping of the helix ends. This calculation assumed the complete exposure of both helix ends to water in the TM state. The ends of our helix backbones appear to be largely shielded from water, as judged from no H/D exchange. The red-shifted NBD fluorescence (Figure 3) may be explained by the lack of the polar "headgroup" in the helix, facilitating water-chromophore interactions as compared with NBD−PE. However, if N−H and C═O groups at the helix ends hydrogen bond to lipid polar groups, the energy cost of transfer of the former groups to the bilayer center will be as high as that in the case of the hydrated helical ends. Other energy barriers for the helix flip-flop include the elastic deformation of the bilayer upon helix tilting (*11*) and the burial of either terminal partial charge, originating from the helix macro dipole, in the membrane (*45*).

Helix−Lipid Interactions. Protein−lipid interactions have been extensively studied using spin-labeled lipids (*33*). In contrast to integral MPs, two-component ESR spectra have rarely been observed in TM peptide systems. For example, TM helicies flanked with tryptophan (*46*) and lysine residues (*5*) did not affect ESR spectra, even at a high peptide-to-lipid ratio of 1/10. Even at a low peptide concentration (2 mol %), our model peptide yielded the motionally restricted component (Figure 5), probably because our ESR measurements were carried out at a lower temperature. These results support lipid perturbation around the helix, that is, a lowering the conformational entropy in the vicinity of a rigid inclusion (*3*, *11*).

Helix−Helix Interactions. Several studies have been carried out on the thermodynamics of glycophorin A TM helix dimerization in detergent micelles using FRET (*24*, *47*,

48). In contrast, there have been few experimental studies in lipid bilayers. Model TM helices have been qualitatively suggested to self-aggregate in lipid bilayers in concentration- and hydrophobic mismatch- dependent manners (*7*, *49*, *50*). Our FRET results could be best explained by a monomer−dimer equilibrium with $\Delta G \sim -13$ kJ/mol (~ 5 *RT*), although some possible errors must be considered. First, the assumption that one acceptor per aggregate completely quenches the donor in the same oligomer may result in underestimation of association. However, this error is not significant because, assuming an interfluorophore distance of 42.5 Å for antiparallel dimer, we obtain a similar value of $\Delta G \sim -14$ kJ/mol. Second, the actual κ^2 value of the **II**−**III** pair might be larger than $^2/_3$, especially when the chromophores are directly labeled at the N-terminus. The FRET results from **II** to TMR−PE could be well described by the Wolber−Hudson equation assuming $\kappa^2 = {}^2/_3$ (Figure 6). In a fluid membrane, the rhodamine fluorophore attached to PE was reported to have a rotational diffusion time on the order of its excited-state lifetime (*51*). The fluorescent anisotropy as a measure of motional freedom of **III** ($\sim$0.18) was even smaller than that of TMR−PE ($\sim$0.2). Furthermore, FRET studies using N-termini-labeled TM or amphipathic helices demonstrated the validity of the $\kappa^2 = {}^2/_3$ assumption (*52*). Errors in the estimation of ΔG are estimated to be 2−3 kJ/mol if various possible errors are taken into consideration; for example, a κ^2 value of 1 or an uncertainty of 3% in the determination of Q are assumed.

van der Waals interactions between tightly packed nonpolar side chains (*47*, *53*) and interactions between polar side chains (*34*, *54*−*56*) are known to drive TM helix association. The fact that our peptide lacking these interactions also weakly self-aggregates suggests the presence of some "basal" driving forces for TM helix association. These forces plausibly include antiparallal helix dipole−dipole interaction, the energy of which has been estimated to be 2−4 *RT* dependent on the extent of shielding of helix ends from water (*13*), in keeping with the absence of self-quenching of NBD fluorescence (Figure 8). Lipid-mediated helix association (1 to several *RT* (*3*, *57*)) as well as, in our particular case, an Ala coil type interaction (*58*) may also contribute to the evaluated ΔG value. Another contribution would be an entropy loss upon dimerization.

The FRET data were most satisfactorily explained by monomer−dimer equilibrium (Figure 7), in keeping with the absence of self-quenching of **II** (Figure 8); aggregates larger than dimer would allow proximity of NBD groups. Dimer formation is probably because (1) larger aggregates would include repulsive dipole−dipole interaction components and (2) lipid-mediated helix association would be lost for larger proteins (*57*). We restricted our analysis at lower peptide contents, where there are enough bulk lipid molecules and the bilayer organization is not significantly perturbed. However, we do not exclude the possibilities that larger aggregates are formed at higher peptide contents and that, even at the lower peptide concentrations used in this study, there was a minor fraction of larger aggregates that did not significantly affect the estimation of aggregation free energy. For further detailed thermodynamic analysis, a pair of fluorescent-labeled peptides that can detect only antiparallel aggregates without significant spontaneous FRET will be required.

APPENDIX

Under the photosteady-state conditions, Q_D is given by

$$Q_D = \frac{k_{em}}{k_{em} + k_{nr}} \tag{A1}$$

k_{em} and k_{nr} represent the rate constants of fluorescence emission and nonradiative decay (other than FRET) processes, respectively. In the presence of cis spontaneous transfer, the quantum yield relative to Q_D is given by using the corresponding rate constant (k_{cis})

$$q_{cis} = \frac{k_{em}}{k_{em} + k_{nr} + k_{cis}} \frac{1}{Q_D} = \frac{k_{em} + k_{nr}}{k_{em} + k_{nr} + k_{cis}} \tag{A2}$$

A similar equation holds for trans spontaneous transfer

$$q_{trans} = \frac{k_{em}}{k_{em} + k_{nr} + k_{trans}} \frac{1}{Q_D} = \frac{k_{em} + k_{nr}}{k_{em} + k_{nr} + k_{trans}} \tag{A3}$$

q_s is deduced from q_{cis} and q_{trans}

$$\begin{aligned} q_s &= \frac{k_{em}}{k_{em} + k_{nr} + k_{cis} + k_{trans}} \frac{1}{Q_D} \\ &= \frac{k_{em} + k_{nr}}{k_{em} + k_{nr} + k_{cis} + k_{trans}} \\ &= \left(\frac{k_{em} + k_{nr} + k_{cis}}{k_{em} + k_{nr}} + \frac{k_{em} + k_{nr} + k_{trans}}{k_{em} + k_{nr}} - \frac{k_{em} + k_{nr}}{k_{em} + k_{nr}} \right)^{-1} \\ &= \left(\frac{1}{q_{cis}} + \frac{1}{q_{trans}} - 1 \right)^{-1} \end{aligned} \tag{A4}$$

REFERENCES

1. Popot, J. L., and Engelman, D. M. (2000) *Annu. Rev. Biochem. 69*, 881−922.
2. White, S. H., and Wimley, W. C. (1999) *Annu. Rev. Biophys. Biomol. Struct. 28*, 319−365.
3. Jänig, F. (1983) *Proc. Natl. Acad. Sci. U.S.A. 80*, 3691−3695.
4. White, S. H., and Wimley, W. C. (1998) *Biochim. Biophys. Acta 1376*, 339−352.
5. Subczynski, W. K., Lewis, R. N., McElhaney, R. N., Hodges, R. S., Hyde, J. S., and Kusumi, A. (1998) *Biochemistry 37*, 3156−3164.
6. Zhang, Y. P., Lewis, R. N., Hodges, R. S., and McElhaney, R. N. (1995) *Biochemistry 34*, 2362−2371.
7. Ren, J., Lew, S., Wang, Z., and London, E. (1997) *Biochemistry 36*, 10213−10220.
8. Killian, J. A., and von Heijne, G. (2000) *Trends Biochem. Sci. 25*, 429−434.
9. Von Heijne, G. (1999) *Q. Rev. Biophys. 32*, 285−307.
10. Killian, J. A., Salemink, I., de Planque, M. R., Lindblom, G., Koeppe, R. E., and Greathouse, D. V. (1996) *Biochemistry 35*, 1037−1045.
11. Ben-Shaul, A., Ben-Tal, N., and Honig, B. (1996) *Biophys. J. 71*, 130−137.
12. Ben-Tal, N., Ben-Shaul, A., Nicholls, A., and Honig, B. (1996) *Biophys. J. 70*, 1803−1812.
13. Ben-Tal, N., and Honig, B. (1996) *Biophys. J. 71*, 3046−3050.
14. Moll, T. S., and Thompson, T. E. (1994) *Biochemistry 33*, 15469−15482.
15. Cohen, C., and Parry, D. A. (1990) *Proteins 7*, 1−15.
16. Matsuzaki, K., Murase, O., Fujii, N., and Miyajima, K. (1996) *Biochemistry 35*, 11361−11368.
17. Bartlett, G. R. (1959) *J. Biol. Chem. 234*, 466−468.

18. Okamura, E., Umemura, J., and Takenaka, T. (1990) *Biochim. Biophys. Acta 1025*, 94−98.
19. Lippert, E., Nägele, W., Seibold-Blankenstein, I., Staiger, U., and Voss, W. (1959) *Z. Anal. Chem. 170*, 1−18.
20. Lakowicz, J. R. (1999) in *Principles of Fluorescence Spectroscopy*, pp 367−394, Kluwer Acadmic/Plenum, New York.
21. Wolf, D. E., Winiski, A. P., Ting, A. E., Bocian, K. M., and Pagano, R. E. (1992) *Biochemistry 31*, 2865−2873.
22. Wolber, P. K., and Hudson, B. S. (1979) *Biophys. J. 28*, 197−210.
23. Kachel, K., Asuncion-Punzalan, E., and London, E. (1998) *Biochim. Biophys. Acta 1374*, 63−76.
24. Adair, B. D., and Engelman, D. M. (1994) *Biochemistry 33*, 5539−5544.
25. Miyazawa, T., and Blout, E. R. (1961) *J. Chem. Phys. 83*, 712−719.
26. Jackson, M., and Mantsch, H. H. (1995) *Crit. Rev. Biochem. Mol. Biol. 30*, 95−120.
27. Goormaghtigh, E., Raussens, V., and Ruysschaert, J. M. (1999) *Biochim. Biophys. Acta 1422*, 105−185.
28. Fraser, R. D. B., and MacRae, T. P. (1973) *Conformation in Fibrous Proteins and Related Polypeptides*, Academic Press, New York.
29. Matsuzaki, K., Shioyama, T., Okamura, E., Umemura, J., Takenaka, T., Takaishi, Y., Fujita, T., and Miyajima, K. (1991) *Biochim. Biophys. Acta 1070*, 419−428.
30. McIntyre, J. C., and Sleight, R. G. (1991) *Biochemistry 30*, 11819−11827.
31. Fery-Forgues, S., Fayet, J.-P., and Lopez, A. (1993) *J. Photochem. Photobiol., A 70*, 229−243.
32. Abrams, F. S., and London, E. (1993) *Biochemistry 32*, 10826−10831.
33. Marsh, D., and Horvath, L. I. (1998) *Biochim. Biophys. Acta 1376*, 267−296.
34. Choma, C., Gratkowski, H., Lear, J. D., and DeGrado, W. F. (2000) *Nat. Struct. Biol. 7*, 161−166.
35. Chattopadhyay, A. (1990) *Chem. Phys. Lipids. 53*, 1−15.
36. Rothschild, K. J., and Clark, N. A. (1979) *Science 204*, 311−312.
37. Haris, P. I., and Chapman, D. (1988) *Biochim. Biophys. Acta 943*, 375−380.
38. Krimm, S., and Dwivedi, A. M. (1982) *Science 216*, 407−408.
39. Kennedy, D. F., Crisma, M., Toniolo, C., and Chapman, D. (1991) *Biochemistry 30*, 6541−6548.
40. Wimley, W. C., and White, S. H. (2000) *Biochemistry 39*, 4432−4442.
41. Jayasinghe, S., Hristova, K., and White, S. H. (2001) *J. Mol. Biol. 312*, 927−934.
42. Lewis, R. N., Zhang, Y. P., Hodges, R. S., Subczynski, W. K., Kusumi, A., Flach, C. R., Mendelsohn, R., and McElhaney, R. N. (2001) *Biochemistry 40*, 12103−12111.
43. Bechinger, B. (2001) *Biophys. J. 81*, 2251−2256.
44. Jayasinghe, S., Barranger-Mathys, M., Ellena, J. F., Franklin, C., and Cafiso, D. S. (1998) *Biophys. J. 74*, 3023−3030.
45. Kessel, A., Schulten, K., and Ben-Tal, N. (2000) *Biophys. J. 79*, 2322−2330.
46. De Planque, M. R., Greathouse, D. V., Koeppe, R. E., II, Schafer, H., Marsh, D., and Killian, J. A. (1998) *Biochemistry 37*, 9333−9345.
47. Fleming, K. G., Ackerman, A. L., and Engelman, D. M. (1997) *J. Mol. Biol. 272*, 266−275.
48. Fisher, L. E., Engelman, D. M., and Sturgis, J. N. (1999) *J. Mol. Biol. 293*, 639−651.
49. Bogen, S.-T., de Korte-Kool, G., Lindblom, G., and Johansson, L. B.-Y. A. (1999) *J. Phys. Chem. B 103*, 8344−8352.
50. Lew, S., Ren, J., and London, E. (2000) *Biochemistry 39*, 9632−9640.
51. Harms, G. S., Sonnleitner, M., Schutz, G. J., Gruber, H. J., and Schmidt, T. (1999) *Biophys. J. 77*, 2864−2870.
52. Gazit, E., and Shai, Y. (1995) *J. Biol. Chem. 270*, 2571−2578.
53. MacKenzie, K. R., Prestegard, J. H., and Engelman, D. M. (1997) *Science 276*, 131−133.
54. Gratkowski, H., Lear, J. D., and DeGrado, W. F. (2001) *Proc. Natl. Acad. Sci. U.S.A. 98*, 880−885.
55. Zhou, F. X., Cocco, M. J., Russ, W. P., Brunger, A. T., and Engelman, D. M. (2000) *Nat. Struct. Biol. 7*, 154−160.
56. Zhou, F. X., Merianos, H. J., Brunger, A. T., and Engelman, D. M. (2001) *Proc. Natl. Acad. Sci. U.S.A. 98*, 2250−2255.
57. Lague, P., Zuckermann, M. J., and Roux, B. (2000) *Biophys. J. 79*, 2867−2879.
58. Gernert, K. M., Surles, M. C., Labean, T. H., Richardson, J. S., and Richardson, D. C. (1995) *Protein. Sci. 4*, 2252−2260.

BI011161Y